A&A 494, 355–360 (2009)
DOI: 10.1051/0004-6361:200810916

Astronomy & Astrophysics

On oscillations found in an active region with EIS on Hinode

E. O'Shea and J. G. Doyle

Armagh Observatory, College Hill, Armagh BT61 9DG, N. Ireland
e-mail: eos@arm.ac.uk
Received 5 September 2008 / Accepted 27 November 2008

ABSTRACT

Aims. Using temporal series (40″ slot) data in the Fe XII 195 Å line from the extreme-ultraviolet imaging spectrometer (EIS) on board the Hinode satellite, we seek to carry out a statistical study of oscillations in an active region.
Methods. Using wavelet techniques, we measure the frequency and duration of oscillations found in the time series data. Stokes I and V data from Hinode's SOT are used to measure photospheric magnetic fields, while an EIS raster is used to provide estimates of LOS velocity and electron density. The measured frequencies are displayed as maps in different bands to aid their analysis.
Results. Oscillations over a broad range of frequencies (2–154 mHz) are found throughout the active region at the temperature of Fe XII (log T = 6.1 K). Oscillations with frequencies between 2–8 mHz are concentrated in bright plage areas, while oscillations of higher frequency preferentially group at the edges of these areas. Evidence is found for harmonics on the boundary of the active region loop, indicating the presence of standing waves. From a measurement of the lengths and electron density of loops appearing in our active region field-of-view (FOV), together with a knowledge of the periods (frequencies) of the oscillations within the area of these loops, we find a magnetic field value of between 12.2 ± 2.08–18.9 ± 3.40 G, assuming standing fast kink waves.
Conclusions. We conclude that waves, which the observed oscillations are signatures of, are common in the active region studied, over a broad range of frequencies. The change in the distribution of the oscillations present at frequencies less than 8 mHz and those at all frequencies above this indicates a variation of the wave mode with frequency, e.g., possibly from slow magnetoacoustic waves in the bright plage regions to fast magnetoacoustic waves at the boundaries of these regions. The preference for higher frequency oscillations to cluster on the edges of regions of high magnetic field is considered indicative of resonant absorption. Based on our measurements of magnetic field, we conclude that the oscillations found by us in the active region loop are fast kink waves.

Key words. Sun: UV radiation – Sun: atmosphere – Sun: corona – Sun: oscillations – Sun: magnetic fields

1. Introduction

Previous studies such as O'Shea et al. (2001) and Ireland et al. (1999) carried out statistical studies of the oscillatory characteristics of active regions using transition region and coronal lines observed with CDS on board the SOHO spacecraft. Here, we seek to carry out a similar statistical study but with the superior temporal resolution and imaging capabilities of the EUV imaging spectrometer (EIS) on board the Hinode spacecraft (Culhane et al. 2007). In this work we will present a global statistical analysis of all intensity oscillations, measured in a Fe XII 195 Å line, present in an active region on the disk. From this statistical study we will seek to identify different wave modes present in the active region and its structures. We note that O'Shea et al. (2001) found evidence for non-compressive (transverse) waves to be more prevalent in coronal lines (at temperatures between Log T = 6.0–6.3 K) than in lower temperatures lines. We also, therefore, seek to find further evidence for these non-compressive waves. From the measured oscillation frequencies (periods), together with the observed physical quantities of loop length, radius and electron density, we will seek to provide estimates of the magnetic field in the corona. We note that Nakariakov & Ofman (2001), using a similar technique to that which will be used by us, obtained values of 13 ± 9 G for global standing kink waves in an active region.

2. Observations and data reduction

The majority of our observations were made using the EUV imaging spectrometer (EIS) on board Hinode. For information on the underlying photospheric magnetic field, we also made use of Stokes I and V data taken by Hinode's Solar Optical Telescope (SOT) (Tsuneta et al. 2008). The EIS time series dataset (eis_l1_20070703_114622.fits) was obtained at 11:46 UTC on the 3rd July 2007 using the 40″ slot. Only 630 of the 1000 time frames were usable and so the total observation time was 630 × 3.14 s (the cadence) ≈33.0 min. The Nyquist frequency is ≈159 mHz.

As solar tracking was turned on, the same region of the Sun was tracked during the total time of the observations. It is known that EIS suffers from pointing jitter so for this reason we carried out a cross-correlation test to see if this jitter, from one time frame to another, was perhaps responsible for the intensity variations (oscillations) seen at high frequencies. The cross-correlation test revealed that the pointing shift between one time frame (slot image) and the next was, in all cases, less than 1 pixel (i.e., sub-pixel) and, therefore, that the jitter is unlikely to be the cause of any of the oscillations measured.

Along with the three standard lines of Ca XVII 192.8 Å, Fe XII 195.1 Å and He II 256.3 Å, five additional lines (Fe X 184.5 Å, Fe XII 186.9 Å, Fe XIII 202.0 Å, Fe XIII 203.8 Å, Fe XV 284.2 Å, and Si VII 275.4 Å) were obtained. (Note that henceforth we will indentify the lines without the following decimal places, e.g., 195 in place of 195.1, etc.) Due to space constraints, we will only discuss the results from Fe XII 195 Å (log T = 6.1 K) in detail here.

The data taken here was observed in a time around 12 UTC where Hinode experiences a "Golden Period", i.e., where the south atlantic anomaly (SAA) does not intercept the spacecraft

orbit, and the effects of cosmic rays are small. For this reason, and together with the automatic cosmic ray removal used with EIS_PREP, we do not expect that cosmic rays have an important effect on our data. To further reduce any possibility that the high frequency oscillations we see are due to transient brightenings of whatever sort, e.g., cosmic rays, etc., we restricted the frequencies chosen to those that showed four or more repeats, e.g., for a frequency of 100 mHz (10 s period) we only selected those oscillations that have a duration in time of 40 s or more.

An EIS raster (eis_l1_20070703_112758.fits) was run at 11:28 UTC on the 3rd July 2007 by stepping, with a 25 s exposure, the 2″ slit 41 times in the X direction. Ten different Transition Region and Coronal lines were observed in this raster but we will only discuss the results from three of these; Fe X 184.5 Å, Fe XII 195.1 Å and Fe XII 186.9 Å. The radiant flux of these three lines, at each position in the raster, was determined by fitting a Gaussian to the line profile, then integrating under it, taking into account the background level and so removing its influence from the measured flux values. From the flux ratio of the Fe XII 186 Å and Fe XII 195 Å lines (186/195), and with theoretical line ratio (vs. density) calculations from the CHIANTI atomic database (Dere et al. 1997; Landi et al. 2006), electron densities were measured. Typical errors in the density are of the order of 5–10%. Effects (see Young et al. 2008) such as the "grating tilt" (an offset of 0.65 pixels was used by us) and the blend of Fe XII 195.12 Å with Fe XII l95.18 Å, which together worked to reduce the measured density by ≈37%, were taken into account and corrected for. We note that the line-of-sight (LOS) velocities used in this work are *relative* velocities, measured relative to a composite line formed by summing together all individual lines at each pixel position along the slit (Y) and at each raster step in X. The LOS velocities were corrected for the effects of orbital motion and the tilt of the EIS slit by using the routine EIS_WAVE_CORR available within the Solarsoft library of routines.

The SOT data was taken very close in time to the EIS raster, at 11:30 UTC on the same day. Stokes I and V data were obtained using the Na I 5896 Å line. Following Chae et al. (2007), line of sight magnetic fields were measured (and calibrated to units of Gauss) using the ratio of V/I and the observationally determined calibration factor of $\beta = 23.5$ kG.

Standard reduction techniques were used to reduce and prepare the data. For example, the standard routine EIS_PREP was used to reduce the EIS data and the routine FG_PREP to reduce the SOT data. The EIS data was not radiometrically calibrated and the radiance data used is in units of data number (DN).

3. Results

In Fig. 1, we show a raster image of the active region, AR 10961, studied in this work. This is a reverse colour image, with the more intense emission shown as black and vice-versa. Note that the FOV of the slot observations intersects a broad loop feature in the bottom righthand corner, which we have marked with a dotted line and an arrow.

In Fig. 2a we plot an example of the type of time series measured by us in this work from a single pixel location. The pixel location ($X = 365''$, $Y = -253''$) is within the area of the slot shown in Fig. 1, on the top edge of the broad active region loop. Overplotted onto the time series in Fig. 2a is the background variation, shown as a thin black line. This background is calculated using a Fourier lo-pass filter set to the frequency cut-off of ≈2 mHz, i.e. we do not allow oscillations with periods larger

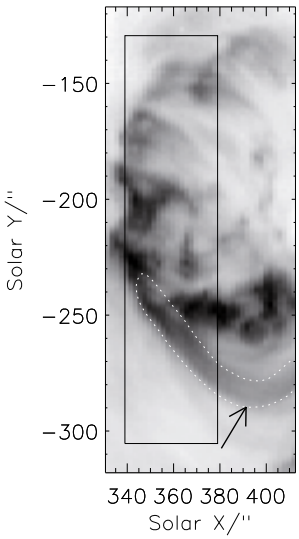

Fig. 1. Raster image of AR 10961 taken in the Fe XII 195 Å line. The FOV of the 40″ slot images is indicated by the black box, and the partial loop by the arrow and dotted black line.

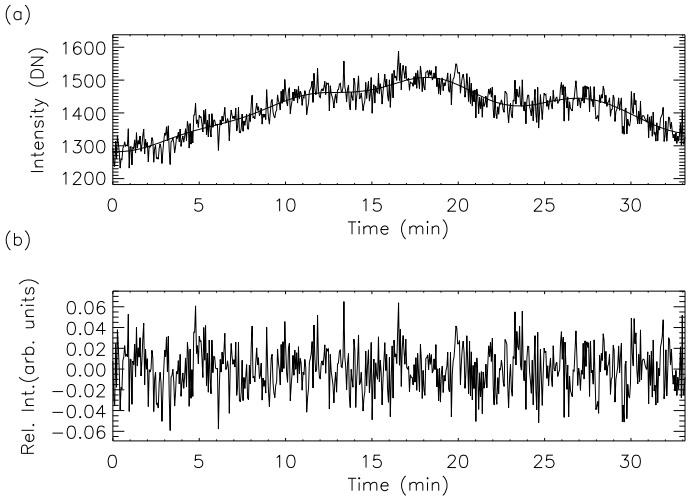

Fig. 2. (a) Time series showing the variation of intensity in a pixel at position $X = 365''$, $Y = -253''$. The solid black line indicates the background intensity. (b) The resulting relative intensity after background removal.

than ≈1/4 of the total observing time. Dividing this background into the original time series (and subtracting a value of 1 from the result) gives us the relative intensity values shown in Fig. 2b. It is the oscillations from these relative intensities that will be measured in this work as they allow us to measure higher frequencies that would otherwise be masked by the bright background.

In Fig. 3 we show four separate examples of the types of oscillations measured by us and their resulting wavelet spectra. We produced the wavelets shown here following the standard prescription given in Torrence & Compo (1998) and the accompanying software[1]. We use a Morlet wavelet transform and a 99.7% (3σ) significance level. In these plots the frequency is cut off at ≈2 mHz due to the removal of the background and the use of relative intensities. The global wavelets to the right of the wavelet spectra show the averaged wavelet spectra results over time. In Fig. 3a, for the time series discussed in Fig. 2, it can be

[1] http://paos.colorado.edu/research/wavelets/software.html

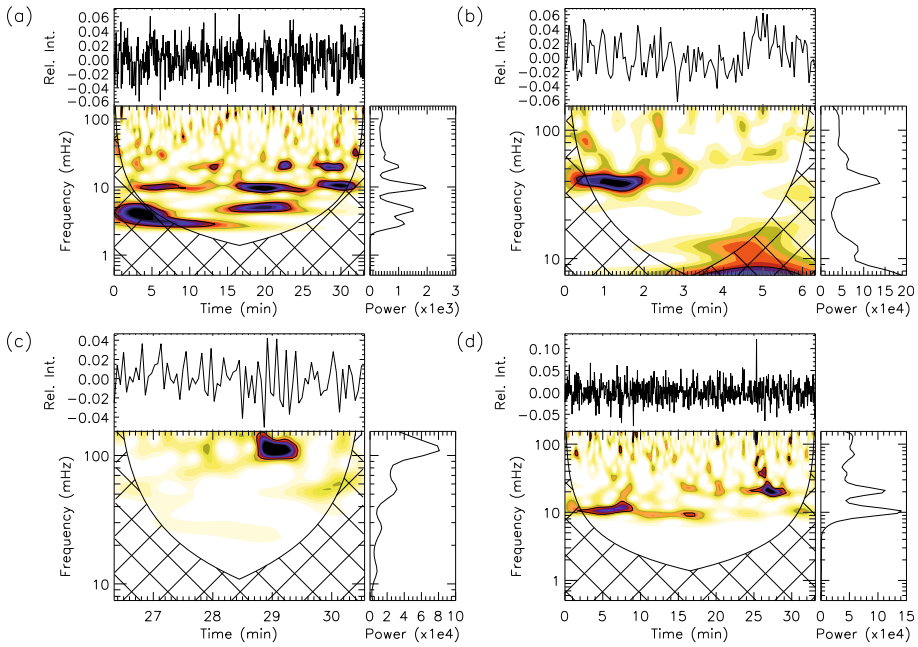

Fig. 3. **(a)** Intensity time series, resulting wavelet spectrum and global wavelet for a pixel at position $X = 365''$, $Y = -253''$ (cf. Fig. 1). The wavelet spectrum is shown in reversed colours, with the darker shades representing higher power. Power above the 3σ level has its boundary indicated by a black enclosing line. **(b)** The same for a pixel at position $X = 364''$, $Y = -255''$. **(c)** The same for a pixel at $X = 364''$, $Y = -256''$. **(d)** The same for a pixel at $X = 368''$, $Y = -256''$.

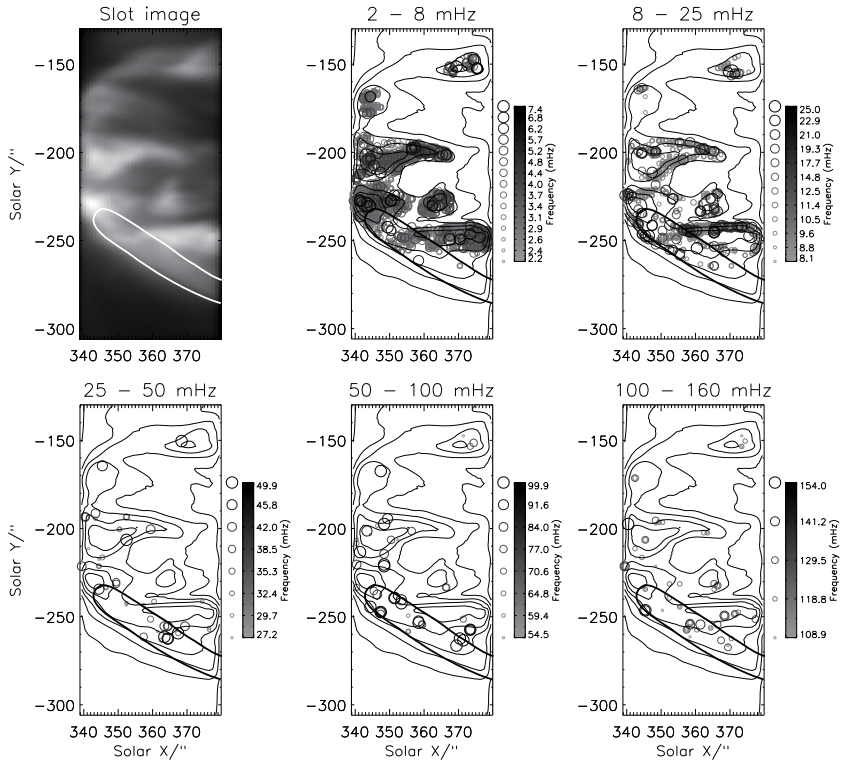

Fig. 4. (*Top left panel*) Radiance image (averaged over all time frames) from the $40''$ slot time series, and frequency maps at different frequency ranges as indicated. The position of the partial loop is indicated by the thick black line in the frequency maps (and the thick white line in the slot image). Note that the radiance image and frequency maps have been slightly stretched in the X direction to aid clarity.

seen that there are oscillations at ≈3, 5, 10 and 20 mHz. We note that this spacing at 5, 10 and 20 mHz is strongly suggestive of harmonics of a standing wave. We further note that the oscillations at ≈3 and 5 mHz, while being significant above the 99.7% significance level, are not included in our further analysis (e.g., Fig. 4) as they do not show four repeats over the lifetime of the oscillation and so fail our strict criterion (as discussed in Sect. 2). In Fig. 3b, from a pixel at $X = 364''$, $Y = -255''$, i.e., within the loop proper, we show oscillations at values of ≈40 mHz. We only show a reduced portion of the time series in this case due to the short time duration of the ≈40 mHz oscillations. We note, however, that, although the oscillations only last for ≈2 min, there is

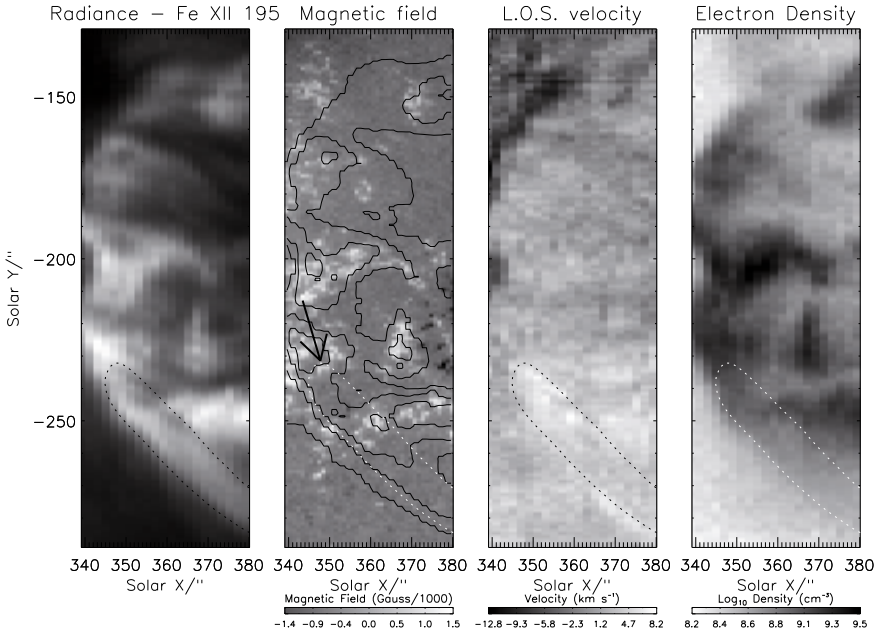

Fig. 5. Images showing, respectively, the Fe XII 195 Å raster, the distribution of photospheric magnetic field (overplotted with the raster radiance contours), LOS velocity and electron density in the observed region. The partial loop is indicated by the dotted lines.

still time in that period for five repeats of the oscillation. This is the advantage of wavelets over Fourier power spectra in this type of analysis as wavelets allow one to follow the evolution of the oscillations over time. In Fourier analysis a high frequency oscillation such as this would likely be averaged out over time and so missed. In Fig. 3c, we show oscillations from pixel location $X = 364''$, $Y = -256''$, again within the active region loop. Here we again show a reduced portion of the time series to show in detail the very high frequency oscillations that are significant (by our criterion) at ≈109 and 118 mHz. Again, we can see that even though, in this case, the oscillations last for less than a minute, they are significant at the 3σ level and obey our strict criterion of at least four repeats over the total time of the oscillation group. In Fig. 3d, we show a final example from pixel location $X = 368''$, $Y = -256''$, on the top edge of the loop. Again, as in Fig. 3a we see evidence for wave harmonics with clear signatures of oscillations at ≈10 and 20 mHz. According to our strict criterion of four repeats, however, only the oscillation at ≈20 mHz is considered in our future analysis. We note the presence of a transient brightening between ≈25–26 min in this time series. This leads to a power reading at a number of high frequencies. However, due to our criterion of four repeats, the high frequency power due to this transient brightening is not considered significant, e.g., it is not included in our future analyses (Fig. 4). All of the above examples have been taken in the active region loop. However, we wish to point out that oscillations in other regions show similar results. It is to be noticed in the results shown here that there is evidence for standing waves (the suggested harmonics) but little evidence for (impulsively generated) travelling waves inside the loop, e.g., in Figs. 3b and c, where, if travelling waves were present, we might expect so see the 'tadpole' structure predicted by Nakariakov et al. (2004). No "tadpole" structure is present in any of the pixels observed in the area of the loop, suggesting that travelling waves are not present in that structure.

In Fig. 4 we show an averaged (over time) radiance image from the $40''$ slot as well as frequency maps of all measured oscillation frequencies. To make the frequency maps more easily readable, the frequencies have been displayed in a number of different frequency bands: 2–8 mHz; 6–25 mHz; 25–50 mHz; 50–100 mHz and 100–160 mHz.

The frequencies in the different plots are plotted as open circle symbols, colour coded and sized according to frequency. We plot the contours of the averaged radiance image in each of the frequency band maps. The area marked out by the solid white line in the radiance image, and the solid black line in the frequency maps, is the location of that part of the active region loop (shown in Fig. 1) that is present in the $40''$ slot. We note that the frequencies shown in these maps were measured using the type of wavelet spectrum plots shown in Fig. 3, at a >99.7% (3σ) significance level. The frequency resolution was limited by the number of wavelet scales (67) chosen.

It is clear from the plot of the 2–8 mHz band that the lower frequencies have a tendency to be situated in locations where the active region plage is brightest. It is likely that these frequencies are similar to the longitudinal oscillations seen in *moss* by De Pontieu et al. (2003), who found periods of 200–600 s (1.7 mHz–5 mHz). As we move to higher frequency bands, e.g, the 8–25 mHz band, it is noticeable that there is a change, with the higher frequencies preferetially situated on the edges of the bright plage regions, e.g., the dense line of frequencies lying along the plage edge at $X \approx 350$–$380''$, $Y \approx -240''$. In the higher frequency bands (the three lower panels), the number of significant oscillations present is much reduced, although a preference for these oscillations to be present along the boundaries of the bright plage is perhaps still visible. The differences in the distribution of the oscillations with frequencies below ≈8 mHz and those with frequencies above this, is indicative of a change in the nature of the waves involved. For example, it could be that there is a change from slow magnetoacoustic waves at frequencies <8 mHz (≈125 s) to fast magnetoacoustic waves at frequencies above this.

Examining the marked area of the loop in Fig. 4, it is noticeable that there are numerous oscillations present in the 2–8 mHz band. These oscillations between ≈3.0–7.4 mHz show clumping along the loop at certain locations, that, as we will see later (cf. Fig. 5), correspond somewhat to areas of strong positive magnetic field. These low frequency oscillations, close to the footpoint of the loop, are possibly linked to photospheric five minute oscillations (typically between ≈2–5 mHz). Looking at the other bands, the loop clearly also contains higher frequency

oscillations between ≈10–141 mHz (≈7–100 s), with clustering occurring at certain locations along the loop, and, in the case of the 8–25 mHz band, preferentially at, or near, the loop edges.

In Fig. 5 we plot images (clipped to the size of the 40″ slot) showing radiance, LOS velocity and electron density from the EIS raster, and magnetic field from the SOT measurements. These images do not have exactly the same FOV in the Y direction as the 40″ slot due to fact that the SOT observations have a shorter FOV in Y. We have, therefore, clipped the EIS raster images in Y to match those of the SOT FOV. It is noticeable that the locations of bright plage in the active region (where the 2–8 mHz oscillations are clustered) are also locations where the magnetic field shows a strong unipolar (positive) field. There is a further correlation in that these plage regions are also the ones that show the largest values of electron density, up to a maximum value of log 9.5 cm^{-3}, as well as the largest values of redshifted LOS velocity, albeit at relatively low values of up to 8.2 km s^{-1}.

The partial active region loop, indicated as a dotted line in these images, has its footpoint (marked by the arrow in Fig. 5) in one of the regions of strong positive magnetic field (≈1500 G). Other strong positive magnetic field regions are clustered further along the length of the loop. The locations of the strong magnetic field within the area of the loop shows some correlation with the locations where we found the majority of the oscillations between ≈3.0–7.4 mHz in Fig. 4.

We note that the active region loop, although appearing as a single broad strand in Figs. 1 and 5, has a more complex structure that is not apparent in the relatively low-resolution EIS raster image (2″ pixels in X, 1″ pixels in Y). To show this more clearly, we plot, in Fig. 6, a TRACE Fe IX/x 171 Å (≈log T = 6.0 K) image (0.5″ pixels in X, 0.5″ pixels in Y) of the active region area, taken at approximately the same starting time as the EIS raster shown in Figs. 1 and 5. Together with this, we plot an EIS Fe X 184 Å (log T = 6.0 K) raster image for comparison, and a Laplacian filtered, edge enhanced, plot of the TRACE 171 Å image data. This Laplacian filtered image is created by convolving the original TRACE image with a Laplacian kernel (Gonzales & Woods 2002). From the TRACE 171 Å image and the associated Laplacian filtered image, it is apparent that what appears as a single loop in the Fe X and Fe XII EIS rasters, is actually five or more thin loop strands. In Fig. 7, we show a larger FOV from the TRACE 171 Å image, allowing us to follow the full length of all the loops of interest. Tracing the loop strands that originate from the same "footpoint", and which approximately correspond in area to the broad illuminated loop seen in Figs. 1 and 5, we produce the white loops shown overplotted on the filtered TRACE image of Figs. 7. We trace five loop strands in total, with lengths of 100″ ± 12.8″ (cross symbols), 113″ ± 17.7″ (triangles), 128″ ± 31.2″ (diamonds), 137″ ± 34.6″ (plusses) and 154″ ± 21.8″ (circles). These lengths were estimated be integrating along the loops, with the uncertainties in the values coming from the uncertainty in the positions of the points in the loop tracing. These five loops correspond to the same area as covered by the illuminated broad loop seen in Figs. 1 and 5, i.e., where oscillations were seen. Other potential loop strands, visible in the TRACE 171 Å Laplacian filtered image, e.g., below ≈−290″ in Fig. 6, are not traced as they are not considered to be responsible for any of the observed oscillations. That is, they are not being illuminated strongly in Fe X 184 or TRACE 171 Å, and are not within the area of the broad illuminated loop seen in Figs. 1 and 5.

We measured a, the radius of the loop cross-section, from a measurement of the cross-section of a number of loops strands

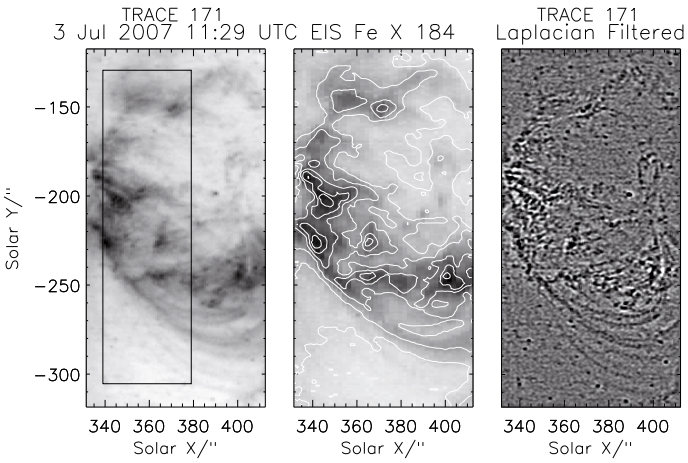

Fig. 6. (*Left*) TRACE 171 Å image, overplotted with the EIS 40″ slot FOV, (*middle*) EIS Fe X 184 Å raster image overplotted with the TRACE 171 Å intensity contours, (*right*) the Laplacian filtered TRACE image.

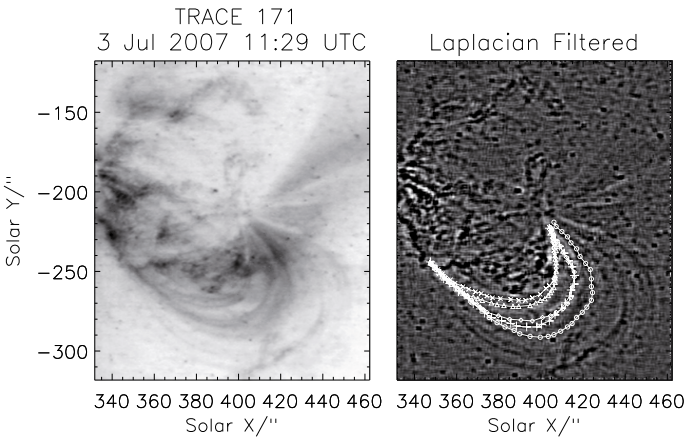

Fig. 7. (*Left*) TRACE 171 Å image showing expanded FOV in X direction (*right*) Laplacian filtered TRACE 171 Å image with the five different loops traced with thin white lines and various indentifying symbols.

and obtained a value of 1.2 ± 0.35″ (8.7 × 10^7 ± 2.5 × 10^7 cm, where 1″ = 725 km).

From the discussion related to Fig. 3 it is likely that standing waves are present in (or on the edge of) the broad active region loop imaged in Figs. 1, 4 and 5. From Roberts et al. (1984), the period of standing slow waves in a coronal loop is given by

$$\tau = C_s L T^{-1/2} \quad (1)$$

where C_s = 1.2 × 10^{-4}, L = the loop length and L = the temperature of the loop (in our case, for Fe XII, the temperature is log T = 6.1 K). The oscillations seen in Fig. 4 could have originated in any of the five loop strands seen in Fig. 7. Therefore the value for L in Eq. (1) must range from 100″ ± 12.8″ (7.25 × 10^9 ± 9.28 × 10^8 cm) to 154″ ± 1.8″ (1.12 × 10^{10} ± 1.58 × 10^9 cm), i.e., between the range of measured loop lengths above. From Eq. (1), these values would suggest a standing slow wave with a period between 7.8 × 10^2–1.2 × 10^3 s (≈0.84–1.3 mHz), which is much larger than anything that can be observed in our data due to the frequency cut-off of ≈2 mHz (≈500 s). For this reason, we cannot rule out the presence of standing slow waves in the loop, but we can say that it is unlikely that any of the oscillations in

the loop with periods higher than 1.3 mHz are due to slow mode standing waves. In reference to Fig. 4, we recall that slow mode waves (slow magnetoacoustic) are, however, likely to be responsible for the oscillations between 2–8 mHz concentrated in the plage regions.

We note that fast kink waves, although essentially non-compressive, may potentially be seen in radiance measurements from the change they can cause on the loop length (Wang & Solanki 2004) or, indeed, just from the angle at which they are observed (Cooper et al. 2003). Taking this into account, we can consider instead that the oscillations we see in the active region loop are fast magnetoacoustic waves. The difficulty of observing the effect of non-compressive waves in intensity measurements may, in fact, explain why there are so few oscillations seen at higher frequencies in our results in general. From the quantities plotted in Fig. 5, and assuming fast magnetoacoustic waves, we can make an estimate of the magnetic field in the active region loop at the coronal temperature of the Fe XII line. We do this by using equations for the standing fast kink waves (Roberts et al. 1984) and the standing fast sausage wave (Aschwanden et al. 2004). For example, from the equation for the standing fast kink wave, we can represent the magnetic field as

$$B_{\rm f} = \frac{C_{\rm f} L N_{\rm e}^{1/2}}{\tau j} \tag{2}$$

and, from the equation for the standing sausage mode ($\tau = 2.62a/V_{\rm A}$), as

$$B_{\rm s} = \frac{2.62 a N_{\rm e}^{1/2}}{2.18 \times 10^{11} \tau} \tag{3}$$

where L is the length of the loop, $N_{\rm e}$ is the electron density within the loop, $C_{\rm f}$ is a constant with a value of 6.5×10^{-12}, j the order of the oscillation harmonic, a is the radius of the loop cross-section, τ is the period (1/frequency) and $V_{\rm A}$ the Alfvén speed, given by $B/\sqrt{4\pi\rho} = 2.18 \times 10^{11} B/\sqrt{N_{\rm e}}$. From Fig. 5, the density in the visible part of the loop can be seen to be higher towards the footpoint, but roughly decreasing outwards. We measure an average density, $N_{\rm e}$ of $6.73 \times 10^8 \pm 3.39 \times 10^7$ cm^{-3} in those parts of the loop visible in Fig. 5, with a maximum value of $1.86 \times 10^9 \pm 7.79 \times 10^7$ cm^{-3} (at the footpoint) and a minimum value of $1.77 \times 10^8 \pm 1.51 \times 10^7$ cm^{-3}. We recall that in Fig. 4 we measured (significant) periods over a broad range of ≈7–333 s (3–141 mHz) within the loop, allowing for the criterion of four repeats, with the oscillations measured at ≈2–5 mHz considered to be the coronal counterparts of 5 min photospheric oscillations. We note, however, that in examining individual oscillations, e.g., in Fig. 3a and d evidence is only found for standing waves at ≈10 mHz (≈100 s) and 20 mHz (≈50 s). Assuming, therefore, that the period of 100 s (≈9.62–10.5 mHz in Fig. 4) is the first harmonic of standing waves in the loop, i.e., assuming j is equal to 1, and using the measured values for L, the average value for $N_{\rm e}$ and a above, we can calculate $B_{\rm f}$ to be between 12.2 ± 2.08–18.9 ± 3.40 G (with the range due to the measured range in the L values) and $B_{\rm s}$ to be 0.27 ± 0.08 G. We take the error in the measured frequencies to be ±10%. Of course, if one instead takes the first harmonic to have a lower value of, say, 5 mHz, e.g. the value also shown in Fig. 3a, which did not fulfil the four repeat criterion, then these estimates of magnetic field must be halved. In addition, if we had instead used the maximum value for $N_{\rm e}$, instead of the average above, the value of $B_{\rm f}$ would be (for a period of 100 s) 20.3 ± 3.41–31.4 ± 5.60 G and $B_{\rm s}$ would be 0.45 ± 0.14 G. Similarly, using the minimum value of $N_{\rm e}$, $B_{\rm f}$ would be 6.26 ± 1.15–9.67 ± 1.87 G and $B_{\rm s}$ would be 0.14 ± 0.04 G. We note that Nakariakov & Ofman (2001) found values for the magnetic field to be between 4–30 G in coronal loops measured by TRACE (for a realistic range of densities, albeit at values higher than those found by us above), which suggests that the value found by us for fast kink waves is more correct. This, in turn, strongly indicates that the high frequency waves we see in the loop are fast kink waves. This is perhaps not too surprising as Aschwanden et al. (2004) reports that fast sausage waves are likely limited to loops, such as flare loops, that possess a high electron density.

4. Discussion and conclusions

We find that oscillations over a large range of frequencies (2–154 mHz) are present throughout the active region at the temperature of Fe XII. Frequencies <8 mHz are preferentially clustered in areas of bright plage with high density, high (photospheric) magnetic field and LOS velocity, while higher frequencies, by contrast, are found preferentially on the edges of this bright plage. We suggest that this indicates a variation of wave mode with frequency, possibly from slow magnetoacoustic in the plage (moss) regions to fast magnetoacoustic waves at the boundaries of these regions. The fact that the higher frequency oscillations, >8 mHz, occur preferentially at the edges of areas of high magnetic field may suggest that they are formed as a result of some form of resonant absorption process. We note that this tallies with an earlier work by (O'Shea et al. 2001) where the tendency of higher frequencies to be present in lower intensity regions (loop boundaries, interloop regions) was also recorded. Using measured physical quantities from within the broad active region "loop" identified in Figs. 1 and 5 (resolved as five individual magnetic strands in Figs. 6 and 7), we estimated magnetic field values assuming fast sausage and fast kink waves. The results indicate, based on previous estimates of magnetic field, that the oscillations found within the active region loop are most likely fast kink magnetoacoustic waves.

Acknowledgements. Hinode is a Japanese mission developed and launched by ISAS/JAXA, with NAOJ as domestic partner and NASA and STFC (UK) as international partners. It is operated by these agencies in co-operation with ESA and NSC (Norway). CHIANTI is a collaborative project involving the NRL (USA), RAL (UK), and the following Univerisities: College London (UK), Cambridge (UK), George Mason (USA), and Florence (Italy). TRACE is a mission of the Stanford-Lockheed Institute for Space Research and part of the NASA Small Explorer program. This work was supported by PPARC grant PP/D001129/1.

References

Aschwanden, M. J., Nakariakov, V. M., & Melnikov, V. F. 2004, ApJ, 600, 458
Chae, J., Moon, Y.-J., Park, Y.-D., et al. 2007, PASJ, 59, 619
Cooper, F. C., Nakariakov, V. M., & Tsiklauri, D. 2003, A&A, 397, 765
Culhane, J. L., Harra, L. K., James, A. M., et al. 2007, Sol. Phys., 243, 19
De Pontieu, B., Erdélyi, R., & de Wijn, A. G. 2003, ApJ, 595, L63
Dere, K. P., Landi, E., Mason, H. E., Monsignori Fossi, B. C., & Young, P. R. 1997, A&AS, 125, 149
Gonzales, R., & Woods, R. 2002, Digital Image Processing, 2nd edition (Prentice Hall publishers)
Ireland, J., Walsh, R. W., Harrison, R. A., & Priest, E. R. 1999, A&A, 347, 355
Landi, E., Del Zanna, G., Young, P. R., et al. 2006, ApJS, 162, 261
Nakariakov, V. M., & Ofman, L. 2001, A&A, 372, L53
Nakariakov, V. M., Arber, T. D., Ault, C. E., et al. 2004, MNRAS, 349, 705
O'Shea, E., Banerjee, D., Doyle, J. G., Fleck, B., & Murtagh, F. 2001, A&A, 368, 1095
Roberts, B., Edwin, P. M., & Benz, A. O. 1984, ApJ, 279, 857
Torrence, C., & Compo, G. P. 1998, Bull. Am. Meteor. Soc., 79, 61
Tsuneta, S., Ichimoto, K., Katsukawa, Y., et al. 2008, Sol. Phys., 74
Wang, T. J., & Solanki, S. K. 2004, A&A, 421, L33
Young, P. R., Watanabe, T., Hara, H., & Mariska, J. T. 2008, ArXiv e-prints, 805